Available online at www.sciencedirect.com
SCIENCE DIRECT®
Journal of the European Ceramic Society 26 (2006) 37–47
www.elsevier.com/locate/jeurceramsoc

An extended two-state model for grain growth during gas phase production of powders

Fulian Qiu[a], Terry A. Egerton[a,*], Ian L. Cooper[b]

[a] *School of Chemical Engineering and Advanced Materials, Bedson Building University of Newcastle, Newcastle upon Tyne NE1 7RU, UK*
[b] *School of Natural Sciences, University of Newcastle upon Tyne, Newcastle upon Tyne NE1 7RU, UK*

Received 19 May 2004; received in revised form 12 October 2004; accepted 16 October 2004
Available online 8 December 2004

Abstract

We have investigated a Monte-Carlo treatment of particle-growth by evaporation–condensation based on a combination of a two-state Potts, or Ising, model with the Metropolis algorithm for the acceptance/rejection of simulated growth steps. The effects of initial size-distribution and lattice occupancy on particle-growth through Ostwald ripening via evaporation–condensation have been explored and the sensitivity of the results to model-parameters, such as interaction energy, temperature and second-nearest-neighbour weightings has been investigated.

From an initial random distribution of particles, the predicted growth follows a square root dependence on time, consistent with well known analytical treatments. When the temperature parameter was examined, a critical temperature T_c was found. Below T_c the rate of particle-growth increased with increasing T; but above T_c the growth-rate decreased with increase in T. The correspondence, in the absence of second-nearest-neighbour interactions, of the computed T_c with the analytically determined value demonstrates the robustness of our procedures.

The effects of evaporation–condensation on the size-distribution, characterized by a mean size $\langle R\rangle$ and r.m.s. deviation δ, have received particular consideration. It is predicted that, for three different initial particle size distributions, with the same initial mean size, growth by evaporation–condensation will lead to convergence of the normalized $\delta/\langle R\rangle$ versus time or $\delta/\langle R\rangle$ versus $\langle R\rangle$ curves. Counter-intuitively, a narrow initial size-distribution is not maintained by particles growing by evaporation–condensation.

Finally, we have developed a simple technique for incorporating diffusive phenomena into this model by incorporating distance dependence into the probability of migration. This has reduced the necessary computational time and enabled us to compare the dependence of the $\delta/\langle R\rangle$ versus $\langle R\rangle$ relationship for different values of the characteristic distance. Remarkably and somewhat unexpectedly, we find that for a wide range of model-parameters the normalized deviation is effectively independent of this characteristic distance.

Keywords: Potts Model; Calcination; Grain Growth; Diffusion; Sintering

1. Introduction

Gas-phase production of nano-particulate powders offers many attractions. The necessary volatile starting materials, e.g. metal halides, are often available and the feasibility of large-scale manufacture is amply demonstrated by the oxidation of titanium tetrachloride vapour

$$TiCl_4 + O_2 \rightarrow TiO_2 + 2Cl_2$$

to produce annually 2–3 million tonnes of titanium dioxide particles (~100 nm radius; 7 $m^2\,g^{-1}$).[1] An analogous process for the production of nano-particulate ZrO_2 has been demonstrated at pilot-plant scale.[2] Nano-particles of alumina, silica and titania (surface area 50–150 $m^2\,g^{-1}$) are produced commercially by flame hydrolysis of their respective

* Corresponding author. Tel.: +44 191 222 5618; fax: +44 191 222 6929.
E-mail address: T.A.Egerton@ncl.ac.uk (T.A. Egerton).

0955-2219/$ – see front matter © 2004 Elsevier Ltd. All rights reserved.
doi:10.1016/j.jeurceramsoc.2004.10.017

chlorides,[3] e.g.

$$SiCl_4 + 2H_2 + O_2 \rightarrow SiO_2 + 4HCl$$

Gas phase processes have been developed for titanium boride,[4] titanium nitride[5] and silicon carbide.[6] All of them offer attractive routes to production of fine particles.

In order to control mean particle-size and size-distribution it is important to understand the mechanisms by which such particles grow. Initially, particle-growth in gas-phase reactors depends on the balance between nucleation and growth by surface reaction. However, once the reactants have been consumed, further growth may occur by the aggregation and subsequent sintering of flocculated parents or by Ostwald ripening—in which evaporation and condensation cause small particles to disappear and larger particles to grow as a result of the greater relative surface energy of the smaller particles—a consequence of their greater specific surface area. Although, the gas phase production of oxide nanoparticles can occur at temperatures close to or above the melting point of the bulk oxides[2,7] little attention has been paid to this particular cause of particle-growth—mainly because of the experimental difficulties inherent in differentiating ripening by evaporation–condensation from aggregation and sintering. Computational modelling provides a method of unravelling the effects of the many growth mechanisms, which contribute to each of the main routes and this paper presents a first step in building such a model.

Although the above paragraphs emphasize growth during powder production, evaporation–condensation plays a part in many other particle-growth processes, including calcination of small particles and the growth of crystals in solution. A specific example of the former is the growth of silver particles supported on TiO_2.[8] More generally, the sintering of metal crystallites on catalyst supports is significantly enhanced by small amounts of chlorine which promote mass transport between particles via volatile chlorides.

In general, the time dependence of the mean grain radius, $\langle R \rangle$, may often be described analytically[9] by the relation

$$\langle R \rangle^n = R_0^n + kt \quad (1)$$

where R_0 represents the mean grain-radius at $t = 0$, k is a constant (with Arrhenius temperature dependence) and n is the order of grain growth. The value of n depends on the growth mechanism and is generally taken to be 2 for transfer across a boundary and 3 for diffusion in the bulk.

In order to extend studies of grain growth beyond the limits of analytical approximations, numerical methods are necessary. In this paper, the evaporation–condensation mediated ripening process is studied by Monte-Carlo simulation on a two-dimensional lattice. A two-state (lattice gas or Ising) model is adopted, corresponding to a specified occupancy of filled and empty sites. The simulation proceeds in a stochastic manner, generating a sequence of configurations of lattice states. Trial states are generated from an initial, normally random, distribution and an exchange between a filled and empty surface site is accepted if there is a resultant decrease in surface energy. If an increase in surface energy results, the move is accepted with a probability given by a Boltzmann factor (Metropolis algorithm[10]). As a result, the larger clusters grow at the expense of smaller ones.

The variables in the analysis include the fractional occupancy of the sites, the nearest neighbour interaction strength J and simulation temperature T (combined within the dimensionless parameter $k_B T/J$, where k_B is the Boltzmann constant), the relative strength of next nearest neighbour interactions and a characteristic distance associated with those accepted exchanges which lower the surface energy.

Specifically, moves which lower the surface energy may be assessed in terms of the separation between the two sites involved, to which a characteristic radius may be applied. If the separation between these sites is less than this characteristic radius, the move is accepted; otherwise it is accepted or rejected on the basis of comparison with a random number. This constraint on the phase space has the effect of incorporating a diffusion distance into the model, i.e. it allows for evaporation–condensation being more probable over short distances than long distances.

1.1. Background

The Potts model[10,11] which treats the evolution of a non-equilibrium discrete ensemble populating a regular lattice was first proposed as a generalization of the Ising model for simulating the critical transitions in magnetic materials and gas–liquid phase transitions in a lattice gas with more than two degenerate states.[10] It has been used in conjunction with the Monte-Carlo method to simulate grain growth and evolution of microstructures during sintering, melting, phase transitions, laser ablation and micromachining.[10,12]

Anderson and co-workers developed a 2D simulation of grain growth and examined the growth kinetics, topology, and local dynamics.[13–15] Tikare et al.[16,17] simulated microstructural evolution and size-distribution during solid state sintering. They found that grain growth kinetics were described by a power law with $n = 2$. In these simulation procedures, the spin state populations are not conserved—a lattice site is selected at random, its state is changed to one of its nearest neighbours' states, and the change is accepted or rejected depending on the outcome of the standard Metropolis procedure. Tikare et al.[16,17] also simulated pore migration (surface diffusion) in solid-state sintering using conserved dynamics, so that the total number of pore sites and grain sites remained constant. A pore site was first selected and a neighbouring grain site was chosen. The two sites were temporally exchanged, with the grain site assuming a new state. Then the standard Metropolis algorithm was again used to accept or reject the move.

Matsubara and co-workers have studied microstructures[18,19] formed by liquid-phase sintering and simulated the microstructure development[20] and compared the results of these simulations with experimental grain growth in AlN

based ceramics.[21,22] Tikare and co-workers have also implemented the Monte-Carlo method to simulate microstructural evolution, size-distribution, grain growth and Ostwald ripening in liquid-phase sintered materials.[23–25] They found grain growth kinetics followed a power law with asymptotic exponent, $n \cong 3$ for different fractions of liquid-phase volume in liquid-phase sintering.[23,24] For cases in which long range diffusion is involved[26,27] (solid–liquid sintering, AB alloy sintering) a site and its neighbour are selected at random. If they belong to different phases, they are allowed to exchange their spins. This can create an isolated spin of phase B, which can randomly walk through the matrix of phase A until it reaches another grain of phase B. The probability is then compared with a random number. Using procedures of this type, Zhang et al.[27] found that the liquid-phase hinders the motion of the grain boundary, and the rate of grain growth in the two-phase case is slower than that in the single phase.

Liu et al.[28,29] studied grain growth and grain boundary segregation in binary alloys. The Ising lattice was used to realize the solute diffusion event via spin exchange and the Potts model was applied to simulate a domain growth event via spin adjustment. Dudek et al.[30] employed Q solid-phase states and a single pore state to simulate late stage sintering in metal powders. They found that for the non-conserved system with low porosity, the kinetics of metal grain growth followed a power law with $n = 2$. The pores inside the bulk grain dissolved according to the Lifshitz and Slyozov[31] evaporation–condensation mechanism. For dilute systems, a power law with $n = 3$ was observed.

2. Description of the model

In this paper, we use an Ising (or two-state Potts) model to simulate grain growth processes such as the growth of a single phase solid at the tail end of a gas phase reaction when there is no further reaction between the solid and gas phases.[3,7] The choice of a two-state model may be justified by the fact that, for TiO_2 prepared by gas phase oxidation, each particle normally consists of only one crystallite, as evidenced by the close correspondence between particle-sizes measured from transmission electron micrographs and crystal-sizes calculated from X-ray line broadening. The two-dimensional simulation domain is discretized as a 400×400 square lattice with periodic boundary conditions. The lattice-occupancy (f) is defined as the ratio of the number of occupied lattice sites (N_0) to the total number of lattice sites (N). We assume a single spin state in the solid phase, with spin state (q) = +1, and one in the surrounding inert gas phase with (q) = −1. Adjacent cells with spin state +1 form a grain, within which there are no boundaries. Adjacent lattice sites with a spin state of −1 form free space in which entities can diffuse from one grain to another. The driving force for grain growth is the reduction of surface energy associated with interface between occupied and empty cells.

The energy under consideration is the surface energy whereby all unlike first-nearest neighbours contribute one arbitrary unit of energy to the system. First and second-nearest neighbours are defined as cells with a common side and common corner, respectively. The total surface energy is

$$E = J \sum_{i}^{N_0} \sum_{j}^{8} [1 - \delta(q_i, q_j)] \tag{2}$$

where δ is the Kronecker delta function such that $\delta(q_i,q_j) = 1$ if $q_i = q_j$ and $\delta(q_i,q_j) = 0$ if $q_i \neq q_j$, where q_i is the state of the grain or empty-site at site i, and q_j is the state of the first-nearest and second-nearest neighbours at site j. The contribution of neighbours to the surface energy can be varied through the first-nearest and second-nearest neighbour weightings (w_f and w_s). Eq. (1) then becomes

$$E = J \sum_{i}^{N_0} \sum_{j}^{4} [1 - \delta(q_i, q_j)] w_f + J \sum_{i}^{N_0} \sum_{j}^{4} [1 - \delta(q_i, q_j)] w_s \tag{3}$$

Throughout the simulations w_f was taken as 1, whilst w_s was allowed to vary between 0 and 1.

In our simulations, the two steps in Ostwald ripening, evaporation–condensation and transport between grains, are simulated independently based on (1) an energy-dependent probability and (2) a distance-dependent probability. In the first case, (a) the state of a randomly chosen surface cell is first checked; then a new surface site with different state is selected, and the total system energy (E_i) is calculated from Eq. (3), (b) state-spin exchange is performed for the chosen sites and the total system energy (E_f) calculated and (c) the difference in energy, ΔE, is calculated using Eq. (4).

$$\Delta E = E_f - E_i \tag{4}$$

(d) The standard Metropolis algorithm is then used to determine whether the exchange is accepted or rejected. A transition probability $p(\Delta E)$ is evaluated using

$$p(\Delta E) = \exp\left(\frac{-\Delta E}{k_B T}\right) \quad (\text{for } \Delta E > 0)$$
$$p(\Delta E) = 1 \quad (\text{for } \Delta E \leq 0)$$

where T is the simulation temperature, which defines the degree of thermal fluctuation in the system. A random number R between 0 and 1 is generated such that if $R \leq p$ (ΔE), the exchange is accepted; otherwise, the original configuration is restored. This permits even some of the jumps associated with a positive energy change to be accepted; it allows for the distribution of energies associated with a specified temperature. The dimensionless parameter $k_B T/J$ is varied from 0 to 2.0. Note that the simulation temperature is not a physical temperature, so that the effect of increasing T is not to increase the 'evaporation' frequency. Consequently, setting $T = 0$ does not eliminate crystal growth; it simply eliminates

thermal fluctuations and ensures the rejection of all steps for which $\Delta E > 0$.

For each jump that is successful on the basis of this first criterion a second criterion-based on a distance-dependent probability (p_d)—may be applied. This may be defined as

$$p_d(d, d_L) = \begin{cases} 1 & (d \le d_L) \\ f(d, d_L) & (d > d_L) \end{cases} \quad (5)$$

where d is the distance between the occupied lattice site (x_1, y_1) and the empty lattice site (x_2,y_2) to which the monomer moves, such that

$$d = \sqrt{(x_2 - x_1)^2 + (y_2 - y_1)^2} \quad (6)$$

d_L, the characteristic distance within which any exchanges which lower the energy are accepted with unit probability, is given by

$$d_L = \frac{d_{max}}{2m} \quad (7)$$

where m is a positive number ($\ge$1). The maximum possible diffusion distance d_{max} is dictated by the dimensions X and Y of the simulation matrix and a factor of 1/2 in Eq. (7) arises from the use of periodic boundary conditions.

$$d_{max} = \sqrt{X^2 + Y^2} \quad (8)$$

In the simplest case, the function $f(d,d_L)$ is 0, such that $p_d(d,d_L)$ is a step function, but the effect of other smoothly varying functions will also be explored.

If d is less than or equal to d_L the move is accepted. If d is greater than d_L, a random number R between 0 and 1 is drawn, and a move for which $p_d(d,d_L) < R$ is accepted; otherwise the move is rejected. Thus, unlike the case of two-phase sintering explored by Tikare et al.,[26] where bulk diffusion was treated by a random walk procedure, we have used a fast algorithm by avoiding attempting unsuccessful moves. We consider this procedure to be acceptable because in our simulations, in contrast to those of Tikare et al.,[26] the occupancy is very low. For the formation of one mole of TiO_2 from $TiCl_4$, one mole of solid TiO_2 ($\sim$20 cm^3) coexists with two moles of chlorine gas ($\sim$40 dm^3).

Time (t) in the simulation is measured in units of Monte-Carlo Steps (MCS) such that 1 MCS corresponds to N attempted exchanges, where N is the total number of lattice sites in the system. During the simulation, the mean grain size $\langle R\rangle$ and r.m.s. deviation δ were recorded, where

$$\langle R\rangle = \frac{\sum_k n_k R_k}{\sum_k n_k}$$

$$\delta^2 = \frac{\sum_k n_k R_k^2}{\sum_k n_k} - \langle R\rangle^2 \equiv \langle R^2\rangle - \langle R\rangle^2 \quad (9)$$

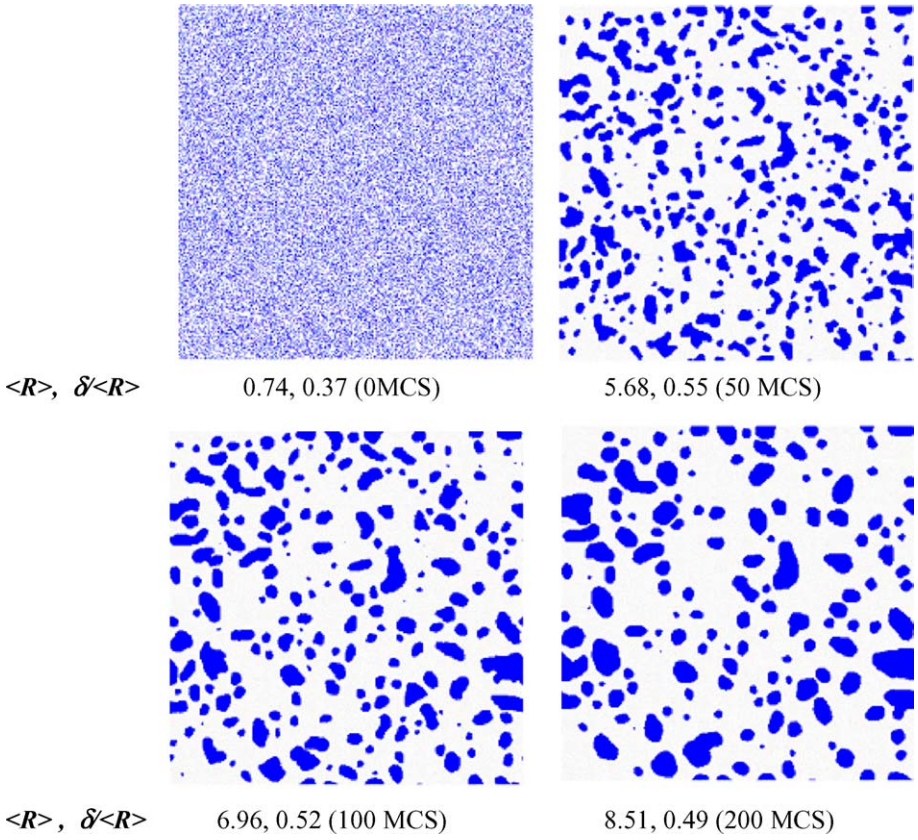

Fig. 1. 'Snapshots' corresponding to an initial random distribution, at 0 Monte-Carlo Steps, and the subsequent growth of particle size, at 50,100 and 200 MCS, for occupancies f = 25%, w_s = 0.5 and k_BT/J = 0. The mean size, the normalized deviation, and the number of MCS are shown below each representation.

Here, the sum is over all grains, where n_k is the number of grains of size R_k.

In the following, all quoted results reflect the average of five runs; 'snapshots' of grain growth are recorded from a typical run in the set.

3. Results and discussion

3.1. Grain growth without distance dependence

The effects of a range of parameters on grain growth were first examined for the case in which the monomer may diffuse (jump) through the whole simulation matrix ($m = 1$). Fig. 1 shows 'snapshots' of the growth during a simulation for an initially random distribution of grains with a lattice occupancy of 25%. The filled cells represent grains. The value of k_BT/J was chosen as 0, implying that any move with $\Delta E > 0$ will be rejected, and for this simulation $w_s/w_f = 0.5$. At $t = 0$, the mean size ($\langle R \rangle$) is 0.74 and normalized deviation ($\delta/\langle R \rangle$) = 0.37. As the simulation progresses, some grains grow at the expense of other grains. After 200 MCS, few small grains remain and many large grains, with a mean size of 8.5 and normalized deviation of 0.49, are seen.

Fig. 2 demonstrates the effects of grid occupancy, second-neighbour weighting, temperature and initial size/size-distribution on the particle-growth. As expected the mean size increases with MCS in all cases. Fig. 2a shows that as the occupancy is increased the 'growth-rate' increases. This effect persists even if the effect of larger R_0 at higher occupancy is compensated for by plotting $\langle R \rangle / R_0$ instead of $\langle R \rangle$ against MCS. The larger fluctuations for MCS > 150 and $f = 40\%$ may be due to coalescence when two or more particles of the decreasing number population come together to form one large particle. For long simulations, when $\langle R \rangle \gg R_0$

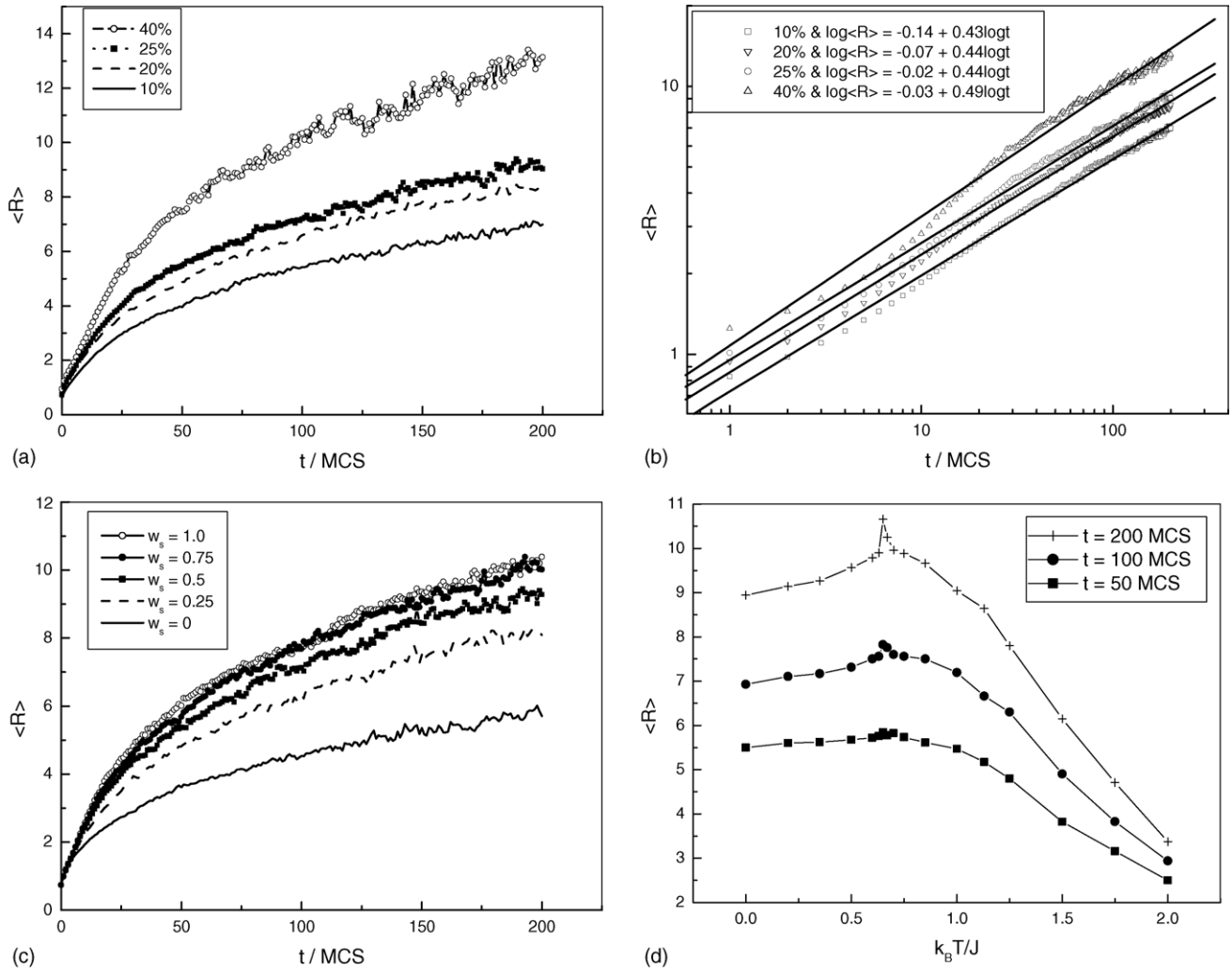

Fig. 2. (a) Mean size vs. time (MCS) for occupancies between 10 and 40% (in all cases $w_s/w_f = 0.5$ and $k_BT/J = 1.0$). (b) The results from (a) plotted on a logarithmic scale to demonstrate the similarity to the behaviour expected from a power law. (c) Mean size vs. MCS for values of w_s from 0 to 1 (in all cases the occupancy, $f = 25\%$ and $k_BT/J = 1.0$). (d) The mean size at 50, 100, and 150 MCS as a function of (k_BT/J) for $w_s/w_f = 0.5$. The discontinuity at (k_BT/J) ≈ 0.67 is clearly seen.

Eq. (1) can be rewritten as

$$\langle R\rangle^n = kt$$

or

$$\log\langle R\rangle = \frac{1}{n}\log k + \frac{1}{n}\log t \tag{10}$$

Fig. 2b displays the curves from Fig. 2a, on a logarithmic scale and demonstrates (except at the early stage of growth) approximate linearity with slopes of 0.43–0.49 for occupancies of 10–40%. The deviation from linearity at less than 10 MCS has been noted previously[26,32] and was attributed to the effect of the initial disorderly lattice structure and neglect of the initial grain radius R_0. Within statistical error, the slopes are in good agreement with the power law prediction $1/n = 0.5$, and confirm the essential robustness of the model.

Fig. 2c shows that mean size increases as second-nearest neighbour weighting increases from 0 to 0.5 and, more slowly, from 0.5 to 1.0. This general trend is intuitively reasonable because an increase in w_s will—through its link to ΔE—increase the relative likelihood of moves from small to large, rather than from large to large, particles. Hence it will increase the growth rate.

Fig. 2d shows the effect on $\langle R\rangle$ of varying T (via k_BT/J at constant J). It is clear the change in growth rate with T is not monotonic, as would be expected in an experimental study at increasing temperatures, but has a turning point at $k_BT_c/J \approx 0.61$. On closer examination of this turning point at longer simulation times (MCS), a discontinuity in gradient of the curve of $\langle R\rangle$ against T at a critical value of temperature (T_c) is observed. This is analogous to an order–disorder phase change, such as that observed in the variation of heat capacity with temperature within the Ising model.

At temperatures below the critical temperature, where $\langle R\rangle$ is observed to increase slightly with increasing T, the energetically favoured increase in grain size is being offset to an increasing extent by the probability of accepting moves which result in an energy increase. At temperatures

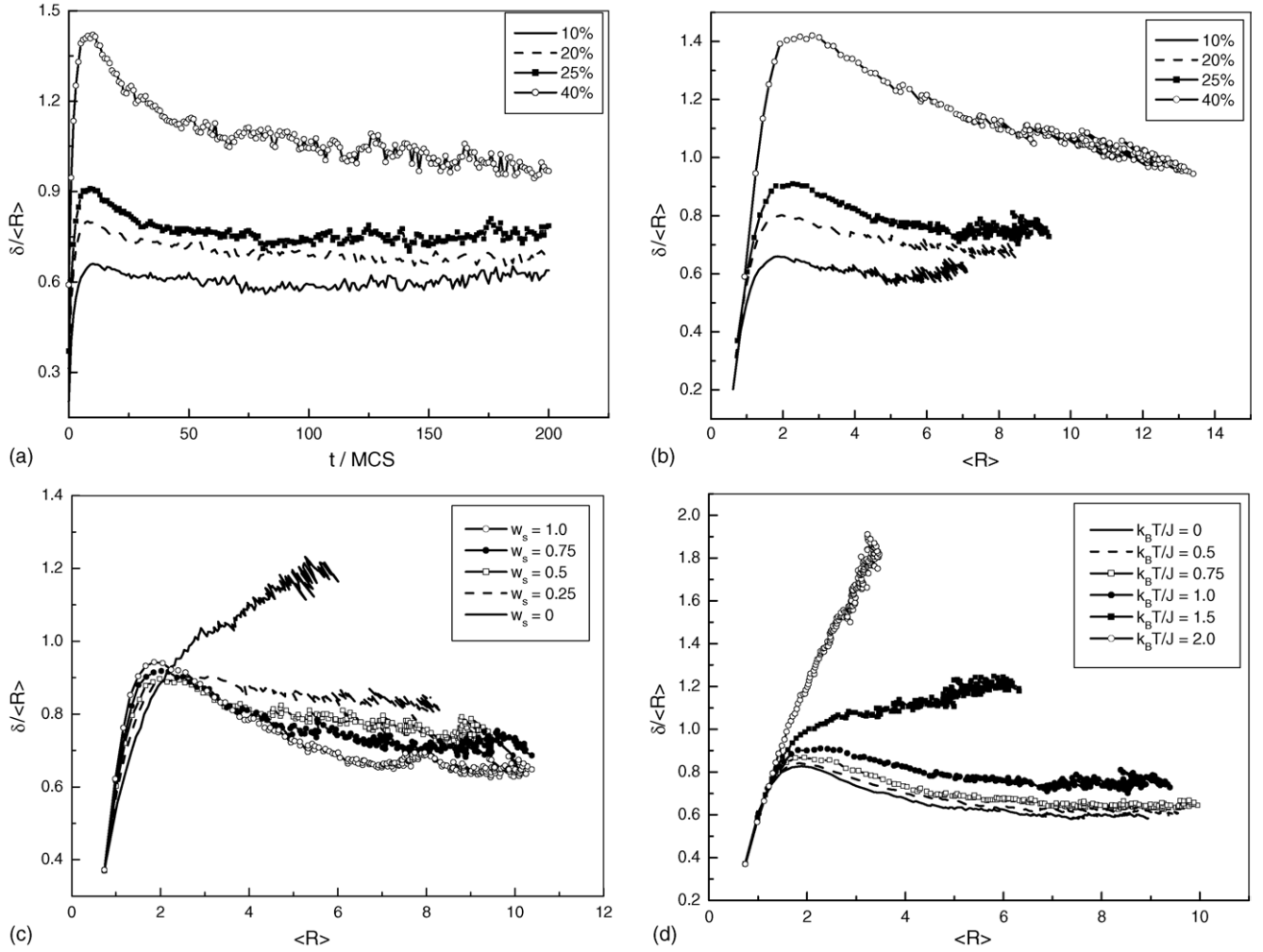

Fig. 3. Normalized deviations as a function of: (a) number of MCS and (b–d) mean size for the cases in Fig. 2. (a) Normalized deviation as a function of time (MCS) for occupancies between 10 and 40% (in all cases $w_s/w_f = 0.5$ and $k_BT/J = 1.0$). (b) Normalized deviation as a function of mean size for occupancies between 10 and 40%.(In all cases $w_s/w_f = 0.5$ and $k_BT/J = 1.0$). (c) Normalized deviation as a function of mean size for values of w_s from 0 to 1 (in all cases the occupancy, $f = 25\%$ and $k_BT/J = 1.0$). (d) Normalized deviation as a function of mean size for (k_BT/J) from 0 to 2.

above the critical temperature, where $\langle R\rangle$ is observed to decrease rapidly with increasing T, the increasing probability of accepting positive energy moves dominates those which result in a lower energy, leading to the break-up of larger grains.

We have also expressed the results of Fig. 2c in logarithmic form, as for Fig. 2a. Some representative slopes derived from these plots are listed in Table 1.

Table 1
The slopes derived from particle-growth curves ($\log\langle R\rangle = a + b \times \log t$) for different second-nearest-neighbour weighting, w_s, temperature, k_BT/J and occupancy, f

w_s[a]	Slope, b[a]	k_BT/J[b]	Slope, b[b]	f[c] (%)	Slope, b[b]
0	0.36	0	0.39	10	0.43
0.25	0.43	0.5	0.42	20	0.44
0.5	0.44	0.75	0.44	25	0.44
0.75	0.46	1	0.43	40	0.49
1.0	0.46	1.5	0.37		
		2	0.25		

[a] $f = 25$, $k_BT/J = 1$.
[b] $w_s = 0.5$, $f = 25$.
[c] $w_s = 0.5$, $k_BT/J = 1$.

The figures in Table 1 confirm the trend indicated in Fig. 2c, namely that the particle-growth-rate increases as second-nearest neighbour weighting increases, and this trend become less pronounced when w_s exceeds 0.75. The inclusion of second-nearest neighbour weightings will on average promote growth by reducing the value of ΔE, and hence lead to $\Delta E < 0$, for a move to a large crystal.

Table 1 also shows that for a fixed value of w_s the particle-growth exponent increases with increasing temperature over a range of temperatures, reaches a peak, and decreases with further increasing in temperature. Hence, it supports the conclusion drawn from Fig. 2d that a critical temperature $k_BT_c/J \approx 0.67$ exists. For the case of $w_s = 0$, with other conditions as before, we obtain a critical temperature of $k_BT_c/J \approx 0.57$ comparable with the value of 0.567 predicted by the lattice gas model.[33] This again shows that our computational procedures are robust.

For some applications of advanced powders a narrow spread of particle sizes is highly desirable. We have, therefore, calculated the standard deviation of the size and normalized this by dividing by the corresponding value of the mean size. Fig. 3a shows that, as f is increased from 10 to 40%, the normalized deviation, $\delta/\langle R\rangle$, first increases with

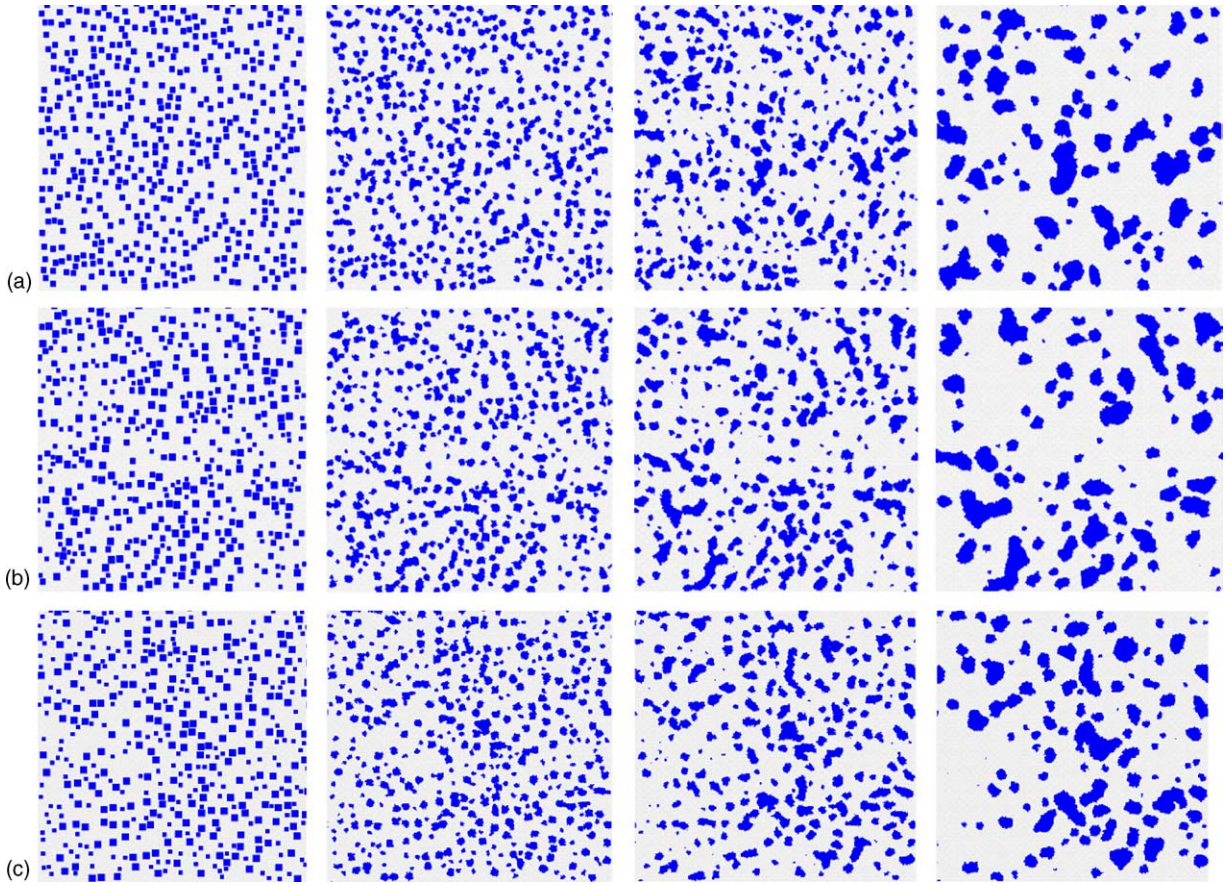

Fig. 4. Snapshots at four different times (0, 10, 50 and 200 MCS) for a fixed initial mean size 4.51 and total occupancy of 20% (a) 8×8 of 0.3125%, (b) 10×10, 8×8 and 6×6 of 0.1% each and (c) 10×10 and 6×6 of 0.15% each.

time (MCS) to a peak value and then gradually decreases to a plateau, Fig. 3a. Normalized deviation, for conditions corresponding to Fig. 2c is shown as a function of mean size in Fig. 3b–d.

Although exceptions to the general pattern occur when $w_s = 0$ (Fig. 3c for which $k_BT/J = 1$) or $k_BT/J > 1.5$ (Fig. 3d for which $w_s = 0.5$) the distribution curves generally display the same pattern. The normalized deviation sharply increases at early stages, goes through a peak, and then decreases as the mean size increases. The initial increase may be attributed to the small particles diminishing in size in order to feed the growth of large particles. Eventually, these small particles disappear completely, and at this stage the size-distribution begins to narrow. However, the broad conclusions from these simulations are that the narrowest size distributions occur in dilute systems (Fig. 3a) and, at long times, further growth by evaporation–condensation does not affect the normalized distribution.

3.2. The effect of initial particle size-distribution on growth

Having established the robustness of the computations and investigated the effects of systematic variation of the input parameters, we can explore the effect of the initial size-distribution on grain growth. Fig. 4, like Fig. 1, shows snapshots of grain growth at different times (0, 10, 50 and 200 MCS). However, instead of the random initial distribution used in Fig. 1 the effect of the breadth of the initial distribution is demonstrated for a fixed initial mean size of 4.51 and an occupancy of 20%. Case (a) corresponds to monodisperse 8×8 particles, the number of particles being equal to 0.3125% of the total number of cells. Case (b) corresponds to equal numbers (0.1% each) of 10×10, 8×8 and 6×6, whilst case (c) corresponds to 0.15% each of 10×10 and 6×6.

Fig. 5 shows the corresponding variations of (a) $\langle R \rangle$ with MCS and (b) normalized deviation with MCS.

Fig. 5a shows that the initial growth of the monodisperse particles is small. Any change from monodispersity must lead to an increase in surface energy and only for $k_BT/J > 0$ can growth occur. A comparison, at $k_BT/J = 1$, of the growth of an initial random distribution with that from a fixed size-distribution shows that grain growth is impaired until a random distribution has been generated. This trend mirrors experimental findings that a narrow initial particle size-distribution substantially slows coarsening rates in the early stages of Ostwald ripening.[34] However, the rate of growth of all three of our artificial populations converges after about 150 MCS as do the $\delta/\langle R \rangle$ versus $\langle R \rangle$ plots (Fig. 5b). These simulations suggest that growth of different initial size distributions by evaporation–condensation will lead to particles with a similar distribution. Evaporation–condensation is predicted to eliminate the differences in size-distribution between an initially random and an initially uniform particle population.

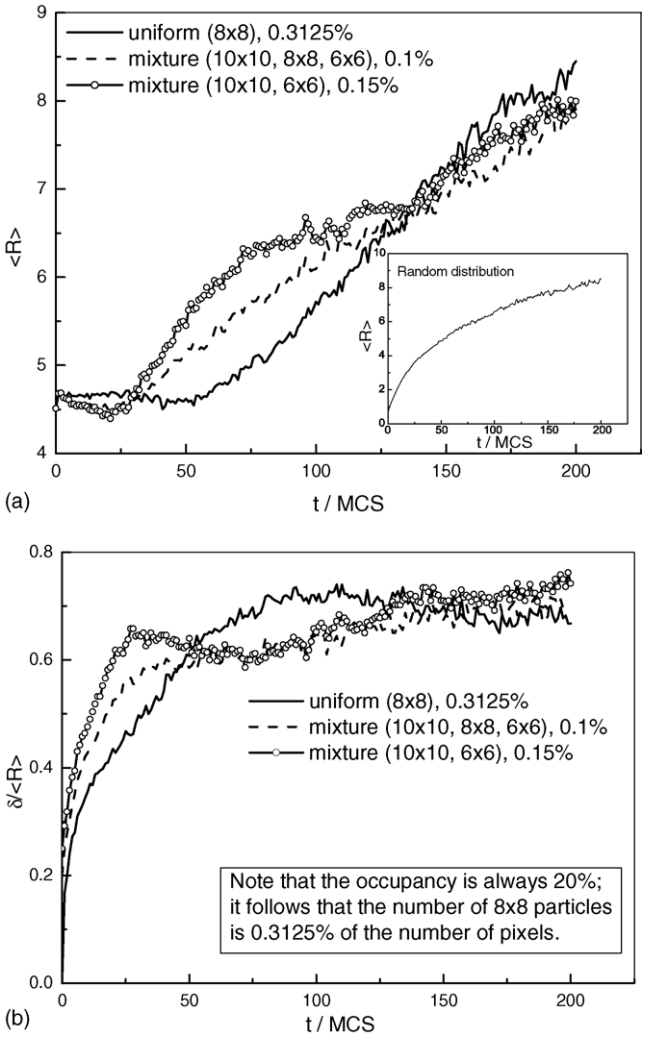

Fig. 5. A comparison of: (a) mean size as function of MCS for the same initial mean size with different initial distributions contrasted with a random distribution (inset). (b) Normalized deviation as a function of MCS for all three cases in Fig. 4.

3.3. Distance-dependent grain growth

The results described in Sections 3.1 and 3.2 are derived on the assumption that condensation may occur at any surface site within the simulation grid and that the probability of condensation does not depend on the distance from the point of evaporation. This corresponds to a thermodynamic analysis. By contrast, consideration of the transport process suggests that condensation is more likely on sites that are near to the point of evaporation. We now turn our attention to this 'distance-dependent' grain growth.

We introduce a characteristic length (d_L) within which all evaporation–condensation steps, which lower the surface energy are accepted. For values of $d > d_L$, a functional dependence is introduced (simple cut-off, exponential decay, Gaussian decay, inverse distance-dependence) whereby evaporation–condensation steps which would automatically lower the energy are only accepted on comparison of the

value of this function with a random number. This allows us to investigate the distance-dependence of the acceptance of evaporation–condensation steps which lower the surface energy. Although we have investigated the effects of a number of functions as noted above, we will concentrate here on the Gaussian decay function

$$g(d_L) = e^{-((d-d_L)/d_L)^2} \quad (11)$$

for $d \geq d_L$ and $g(d_L) = 1$ for $d < d_L$.

This ensures that both the function and its first derivative are continuous at $d = d_L$. It turns out in practice that the various functions yield very similar results and we will only quote results using the above Gaussian function (Fig. 6).

The 'snapshots' (a) to (c) in Fig. 7 at $t = 200$ MCS (all for $f = 40\%$, $w_f = 1$, $w_s = 0.5$) demonstrate that decreasing the diffusion-related characteristic distance $d_L (f = d_{max}/m)$ (i.e. by increasing m) decreases the rate of particle-growth. Correspondingly, the snapshots in Fig. 7d–f, show that increasing times (50, 82 and 153 MCS respectively), are necessary to reach a fixed mean size as the diffusion distance decreases. Conceptually, limiting the distance through which 'monomer' can be transported must decrease the chance of a successful evaporation–condensation step. When the transport distance is very small in comparison with mean

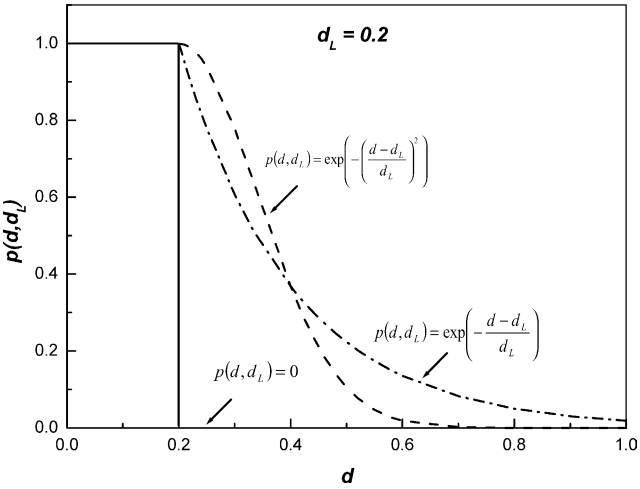

Fig. 6. The variation with distance, d, of various functions used in the calculation of the distance-dependent probability of a move.

inter-particle distance, intra-particle transport will dominate. High energy surface cells will move to a lower energy location on the same particle, i.e. transport will lead to changes in shape rather than size.

The particle-growth curves are plotted in Fig. 8a. It can be seen that shorter characteristic distances (larger values

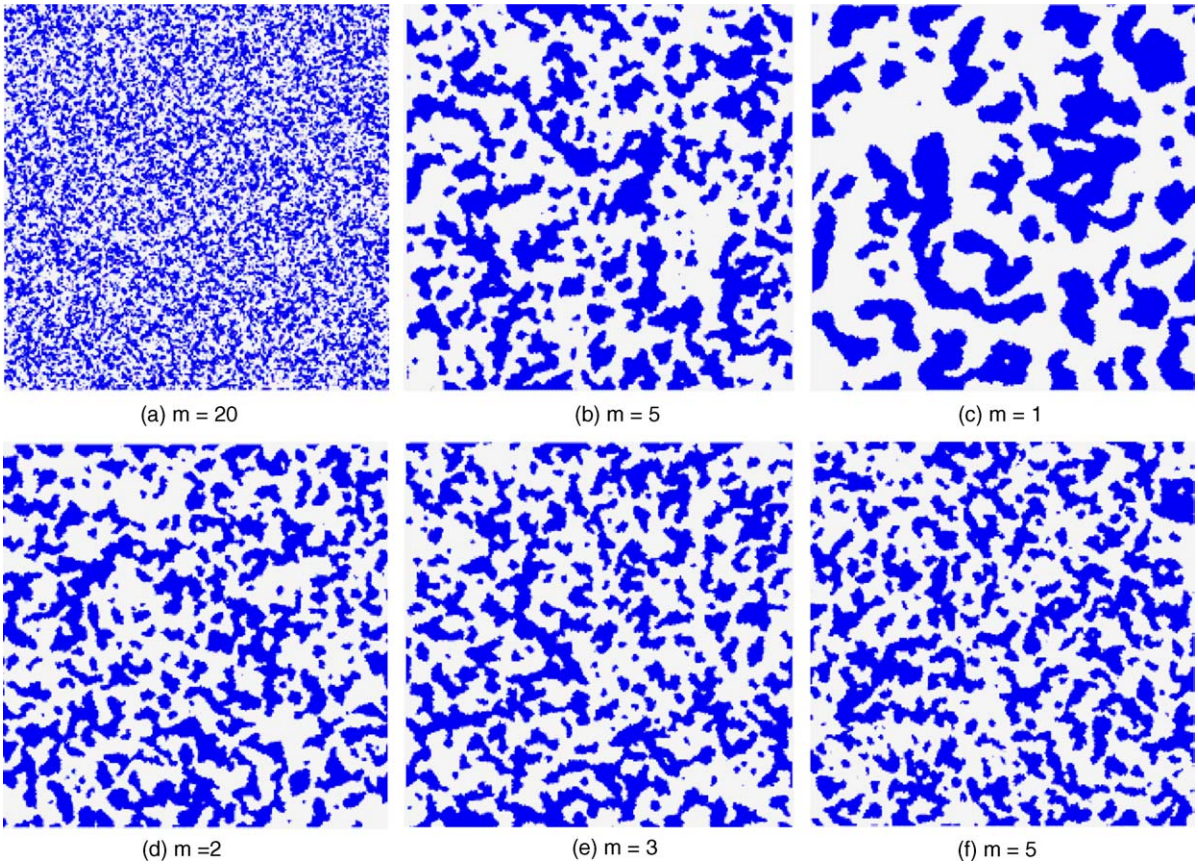

Fig. 7. Snapshots at 200 MCS (a)–(c), and fixed mean size (d)–(f) for different characteristic distances for a case of $f = 40$, $w_s = 0.5$ and $k_B T/J = 1.0$.

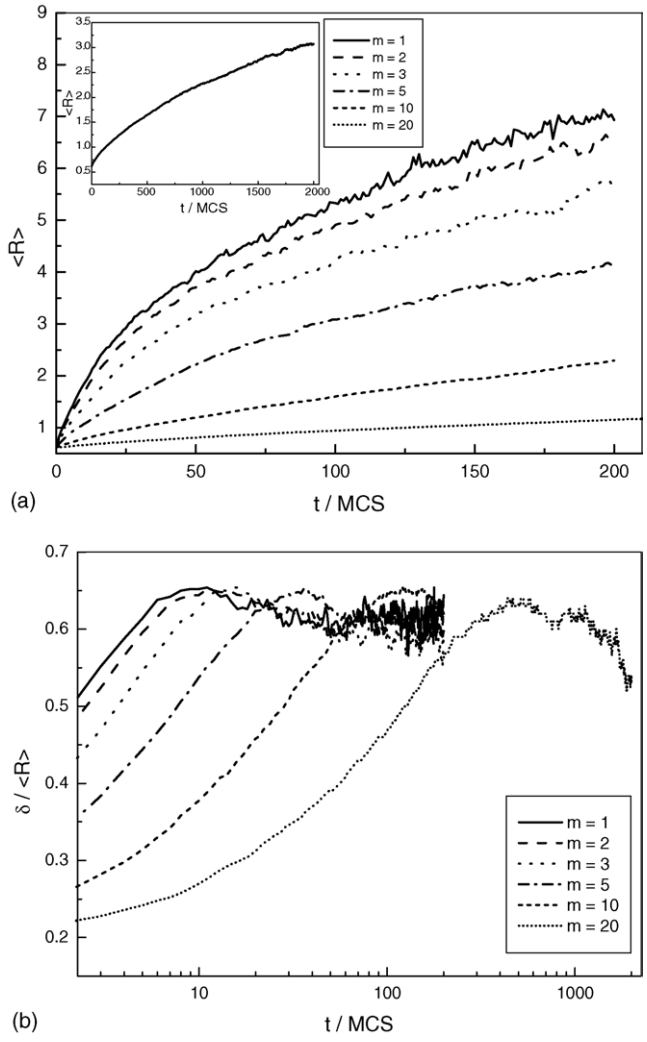

Fig. 8. The effect of decreasing characteristic distance, increasing m, on particle-growth ($f = 10\%$, $w_s = 0.5$ and $k_B T/J = 1.0$ in all cases). (a) Mean size as a function of MCS and (b) normalized deviation as a function of MCs, plotted on a logarithmic scale.

of m) significantly slow the earlier stage of particle-growth. However, for longer times a power-law with exponent 2.0 still holds. This is because at an early stage, when more small grains exist, the majority of moves are energetically favourable, and consequently many energetically-successful moves are rejected by the diffusion limitation; the diffusion restrictions dominate. By contrast, at longer times there are fewer small particles and fewer moves are successful energetically. Consequently, the relative importance of diffusion limitation decreases and the power-law behaviour is re-established.

The corresponding plots of normalized deviation versus with MCS are shown in Fig. 8b. The normalized deviations first go through a maximum, shifting to longer times as d_L decreases. The peak heights are identical for different diffusion distances because similar initial conditions were employed.

Fig. 9 shows normalized deviation as a function of mean sizes for different diffusion distances and $f = 10\%$.

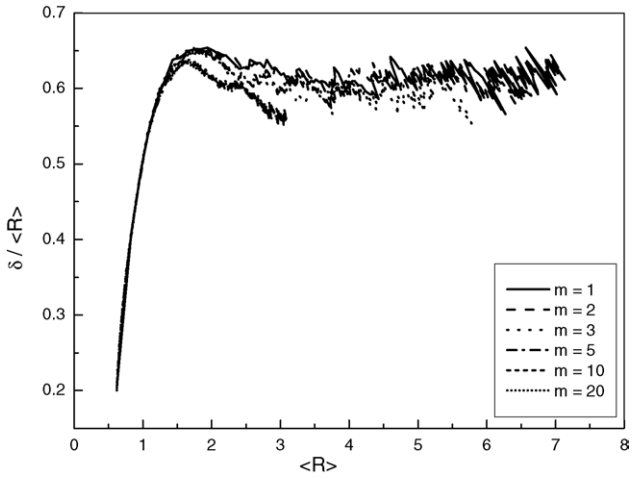

Fig. 9. Normalized deviation as a function of mean size for the same conditions as Fig. 8.

Remarkably, a universal curve was obtained regardless of the diffusion distances. Therefore, these results suggest that the normalized deviation is independent of particle concentration density in the simulation domain. Similar behaviour, not shown here, was observed for a higher occupancy of 40%. Similar universal curves were obtained for the other functions shown on Fig. 6.

4. Conclusions

As stated in the introduction, evaporation–condensation is one mechanism, which can contribute to the growth of particles and may be an important contribution to particle-growth in the later stages of gas-phase powder production. In these processes, not only the rates of particle-growth, but also the size-distribution, which develops, are important. For example, the opacity of TiO_2 pigment and the fracture of oxide ceramics are both affected by the size-distribution of the powders. Therefore, the key conclusions from this study concern the insights with respect to the contribution of evaporation–condensation to the evolution of the size-distribution.

The simulations lead to two such insights. The first is that for growth by evaporation–condensation the ultimate value of normalised size-distribution may be independent of the initial size-distribution of the particles. The second is that the normalised deviation distribution does not depend on the characteristic distance. However, because evaporation–condensation is only one mechanism by which particles can grow, our simulation may only tell part of the story. This model is the first stage in a programme designed to take into account the main mechanistic steps responsible for particle-growth and will, in future work, be combined with models of other processes—specifically a multi-state model of growth by boundary diffusion.

Acknowledgements

This work was carried out within the ACORN programme of the IMPACT Faraday Partnership supported the UK Department of Trade and Industry and EPSRC. We are particularly grateful the sponsorship of Huntsman Tioxide, and for the collaborations of Mr. Mike Westwood and Dr. John Edwards of Huntsman Tioxide.

References

1. Egerton, T. A., Titanium Compounds. In *Kirk Othmer Encyclopedia of Chemical Technology (Vol 24, 4th ed.)*. John Wiley & Sons, New York, 1997. pp. 226–274.
2. Dransfield, G. P., Fothergill, K. A. and Egerton, T. A., The use of plasma synthesis and pigment coating technology to produce an yitria stabilized zirconia. In *Euro Ceramics (Vol 1)*, ed. G. Dewith, R. A. Terpstra and R. M. Metsalaar. Elsevier Applied Science Publishers, London, 1989, pp. 275–279.
3. Deller, K., Ettlinger, M., Fischer, S. and Weinland, R., *Eur. Cosmet.*, 1991, **57**, 391.
4. Edd, J. F., U.S. Patent 4 022 872 (to Alcoa).
5. Blackburn, S. R., Egerton, T. A. and Jones, A. G., Vapour phase synthesis of nitride ceramic powders using a DC plasma. *Br. Ceram. Proc.*, 1991, **47**, 87–94.
6. Fauchais, P., Boudrin, E., Caudert, J. F. and McPherson, R., In *Topics in Current Chemistry (Vol 107)*, ed. S. Venprek and M. Venugoplan. Springer, Berlin, 1983, pp. 59–183.
7. Egerton, T. A. and Fothergill, K. A., Finely divided alumina and its manufacture. *U.K. Patent 2 182 650* (to Tioxide).
8. Lai, X., St. Clair, T. P. and Goodman, D. W., Oxygen-induced morphological changes of Ag nanoclusters supported on TiO_2(1 1 0). *Faraday Dis.*, 1999, **114**, 279–284.
9. Hillert, M., On the theory of normal and abnormal grain growth. *Acta Metall.*, 1965, **13**, 227–238.
10. Binder, K. and Heerman, D. W., *Monte Carlo Simulation in Statistical Physics* (*4th ed.*). Springer, Berlin, 2002, p. 99.
11. Wu, F. Y., The Potts model. *Rev. Mod. Phys.*, 1982, **54**, 235–268.
12. Tikare, V., Miodownik, M. A. and Holm, E. A., Three-dimensional simulation of grain growth in the presence of mobile pores. *J. Am. Ceram. Soc.*, 2001, **84**, 1379–1385.
13. Srolovitz, D. J., Anderson, M. P., Grest, G. S. and Shani, P. S., Grain growth in two dimensions. *Scripta Metall.*, 1983, **17**, 241–246.
14. Sahni, P. S., Grest, G. S., Anderson, M. P. and Srolovitz, D. I., Kinetics of the *Q*-state Potts model in two dimensions. *Phys. Rev. Lett.*, 1983, **50**, 263–266.
15. Anderson, M. P., Srolovitz, D. J., Grest, G. S. and Sahni, P. S., Computer simulation of grain growth—I. Kinetics. *Acta Metall.*, 1984, **32**, 783–791.
16. Tikare, V. and Holm, E. A., Simulation of grain growth and pore migration in a thermal gradient. *J. Am. Ceram. Soc.*, 1998, **81**, 480–484.
17. Tikare, V. and Cawley, J. D., Application of the Potts model to simulation of Ostwald ripening. *J. Am. Ceram. Soc.*, 1998, **81**, 485–491.
18. Matsubara, H. and Brook, R., Computational modeling of mass transfer for ceramic microstructure. Ceramic transactions—mass and charge transport in ceramics. *Am. Ceram. Soc. Bull.*, 1996, **71**, 403–418.
19. Iwamoto, Y., Shin, S. G. and Matsubara, H., Grain growth behaviour of ceramics under the existence of a liquid phase. Ceramic transactions—mass and charge transport in ceramics. *Am. Ceram. Soc. Bull.*, 1996, **71**, 483–490.
20. Matsubara, H., Computational modeling of ceramic microstructure by MC and MD—aspects in dynamic, key engineering materials. *Ceram. Soc. Jpn.*, 1999, **166**, 1–8.
21. Tajika, M., Matsubara, H. and Rafaniello, W., Experimental and computational study of grain growth in AlN based ceramics. *J. Ceram. Soc. Jpn.*, 1997, **105**, 928–933.
22. Tajika, M., Matsubara, H. and Rafaniello, W., Use of computer simulation to aid the understanding of microstructural changes observed in heat-treated AlN ceramics. *J. Ceram. Soc. Jpn.*, 1999, **107**, 1156–1159.
23. Tikare, V. and Cawley, J. D., Numerical simulation of grain growth in liquid phase sintered materials—I. Model. *Acta Mater.*, 1998, **46**, 1333–1341.
24. Tikare, V. and Cawley, J. D., Numerical simulation of grain growth in liquid phase sintered materials—II. Study of isotropic grain growth. *Acta Mater.*, 1998, **46**, 1343–1356.
25. Tikare, V., Holm, E. A., Fan, D. and Chen, L.-Q., Comparison of phase-field and Potts models for coarsening processes. *Acta Mater.*, 1999, **47**, 363–367.
26. Solomatov, V. S., El-Khozondar, R. and Tikare, V., *Phys. Earth Planet. Interiors*, 2002, **129**, 265.
27. Zhang, D.-L., Weng, G.-A., Gong, S.-P. and Zhou, D.-X., The kinetics of initial stage in sintering process of $BaTiO_3$-based PTCR ceramics and its computer simulation. *Mater. Sci. Eng. B*, 2003, **99**, 88–92.
28. Liu, J.-M., A Monte-Carlo approach to domain boundary precipitation in binary alloys. *J. Appl. Phys.*, 1998, **84**, 6582–6587.
29. Liu, J.-M. and Liu, Z. G., Phase precipitation on grain boundaries in binary alloys: a Monte-Carlo approach. *Solid State Commun.*, 1998, **105**, 517–521.
30. Dudek, M. R., Gouyet, J.-F. and Kolb, M., Q + 1 state Potts model of late stage sintering. *Surf. Sci.*, 1998, **401**, 220–226.
31. Lifshitz, I. M. and Slyozov, V. V., The kinetics of precipitation from supersaturated solid solutions. *J. Phys. Chem. Solids*, 1961, **19**, 35–50.
32. Holm, E. A., Glazier, J. A., Srolovitz, D. J. and Grest, G. S., Effects of lattice anisotropy and temperature on domain growth in the two-dimensional Potts model. *Phys. Rev. A*, 1991, **43**, 2662–2668.
33. Onsager, L., Crystal statistics. I. A two-dimensional model with an order–disorder transition. *Phys. Rev.*, 1944, **65**, 117–149.
34. Fang, Z. G. and Patterson, B. R., Experimental investigation of particle size-distribution influence on diffusion controlled coarsening. *Acta Metall.*, 1993, **41**, 2017–2024.